Computer Assisted Mechanics and Engineering Sciences, 7: 307–320, 2000.
Copyright © 2000 by Institute of Fundamental Technological Research, Polish Academy of Sciences

Finite element analysis of the action of buoyancy-induced and thermocapillary flow on the melting of tin in a 2D square cavity

Marc Medale, Marc Jaeger and Ahmed Kaiss
IUSTI-CNRS UMR 6595, Université de Provence,
Technopôle de Château-Gombert, 5 rue Enrico Fermi, 13453 Marseille Cedex 13, France

(Received August 26, 1999)

A finite element model has been developed for the computation of melting/solidifying process under the combined action of buoyancy and surface tension forces. Validated on the square cavity benchmark of Gobin and Le Quéré (Bertrand *et al.* [3], Gobin and Le Quéré [17]), the numerical model is used to extend this previous analysis to the free surface case where surface tension can drive the flow (capillary flow). A comparison of the results obtained for three types of boundary conditions applied at the top of the melting pool is performed. It shows that in the studied case of tin where the thermal Bond number is moderated ($Bo = 200$), the flow is still mainly dominated by buoyancy effect as long as the melted pool is deep enough like in the square cavity case of the above mentioned benchmark.

Keywords: phase change (melting, freezing), natural convection (buoyancy, thermocapillary flows), incompressible Navier–Stokes equations, finite element method

NOTATIONS

Fo – Fourier number	γ – Surface tension coefficient
Ste – Stefan number	L_F – Latent heat of melting
Pr – Prandtl number	α – Thermal diffisivity
Ra – Rayleigh number	t – Time
Ma – Marangoni number	H – Height of the cavity
Bo – Thermal Bond number	u – Velocity vector
ρ – Density	p – Pressure
μ – Dynamic viscosity	T – Temperature
β – Volumetric expansion coefficient	q – Heat flux
C_P – Specific heat coefficient	g – Gravity acceleration vector
k – Thermal conductivity	f_L – Volumic liquid fraction

1. INTRODUCTION

It has been established that fluid motion has a great impact on the heat transfer during melting or solidification, as well as on the morphology of the solid-liquid front (Fleming [14], Viskanta [43], Gau and Viskanta [15]). The mechanisms leading to bulk fluid motion during phase transformation are (Kobayashi [26], Viskanta [43]):

- natural convection induced by thermal gradient or/and solute gradient;
- shrinkage due to the density differences between the solid and liquid phases;
- thermocapillary or/and solutcapillary forces, in the presence of a free surface.

One must add to this list the driving forces specific to each industrial process, like rotation induced forces in industrial crystal growth processes (Jones [22]) or electromagnetic forces in welding (Oreper and Szekely [32]). Sometimes, these forces are applied to stabilize the fluid motion, but they must be taken into account in the analysis if present.

Most today analysis of solid-liquid phase change problems take into account natural convection. For a review, see Samarskii *et al.* [34] or more recently Voller [45].

Shrinkage-induced convection becomes important in the absence of other mechanism for sustaining liquid flow. It has been studied by Chiang and Tsai [8] and has been also taken into account by Voller and Sundarraj [47] in their analysis of inverse segregation.

In order to understand the basic mechanisms of heat transfer and fluid flow occuring during the melting process, combined action of buoyancy and thermocapillary force has been investigated by many authors without phase change and in simplified geometry (Kirdyashkin [25], Villers and Platten [41, 42], Carpenter and Homsy [6], Ben Hadid and Roux [20], Gouesbet *et al.* [18], Shyy and Chen [37]). In the last years, some studies have also incorporated the deformation of the free surface (Brown *et al.* [5], Sasmal and Hochstein [35], McClelland [30], Chippada *et al.* [9], Cliffe and Tavener [10]). However, very few works have focussed on the action of surface tension forces on solid-liquid phase change processes. Actually, most of the studies have been undertaken for weld pool in welding processes or surface processing, where surface tension is the dominant driving mechanism (Oreper and Szekely [32], Chan *et al.* [7], Kou and Wang [27], Basu and Srinivasan [1], Hsu and Rubinsky [21], Tsai and Kou [40], Zacharia *et al.* [49], Ravindran *et al.* [33]). From the phase transformation point of view the problem is then simplified by the fact that the stationary regime is quite reached. On the other hand, the problem is a challenging one because of the complicated shape of the free surface (Keanini and Rubinsky [24], Medale and Jaeger [31]). In systems of crystal growth from the melt, the importance of studying the influence of surface tension forces has been pointed out by Schwabe [36]. Computations have mostly focussed on the thermocapillary flow in a melt column between two heating or sample rods (see Lan and Kou [28] and references therein). Katsumura *et al.* [23] have studied numerically the melting of metal by induction heating in an axisymmetric configuration taking into account the deformation of the free surface. Liu *et al.* [29] have investigated numerically the melting as well as solidification of a pure medium (of low and moderately high Prandtl number) in a 2D rectangular cavity heated from one side under the combined action of buoyancy and surface tension forces. However, as noticed by the latter authors, solutcapillary forces oppose thermocapillary forces in most liquids. Thus, the importance of thermocapillary convection depends on the degree to which solutcapillary effects are present within the system. They conclude finally that "regardless of the uncertainty associated with surface effects, the actual phase change behavior is likely to be bracketed by the limiting cases represented by the effective no-slip and pure thermocapillary treatment of the liquid surface boundary condition".

In the frame of the benchmark proposed by Gobin and Le Quéré (Bertrand *et al.* [3], Gobin and Le Quéré, [17]), on the melting of pure medium (tin and octadecane) in a 2D rectangular cavity, only no slip boundary condition is considered. The aim of the present study is to extend the analysis of this problem when the upper boundary is a free surface instead of a rigid wall. Two kinds of free surface boundary conditions are considered, namely perfect slipping and thermocapillary conditions. The medium under consideration is tin.

2. Problem definition

The global description of the problem under consideration is given in the definition of the benchmark (Bertrand *et al.* [3], Gobin and Le Quéré, [17]). A 2D square cavity (height H = width $L = 0.1$ m) is filled with solid tin at the solidus temperature $T_F = 232°C$. At the initial time, the temperature of the left vertical wall is raised up to a value $T_1 = 235°C$, while the other vertical wall is maintained at the initial temperature. The horizontal walls are assumed to be adiabatic. In the benchmark, both are rigid walls with a no-slip boundary condition. In the present study, the liquid upper horizontal

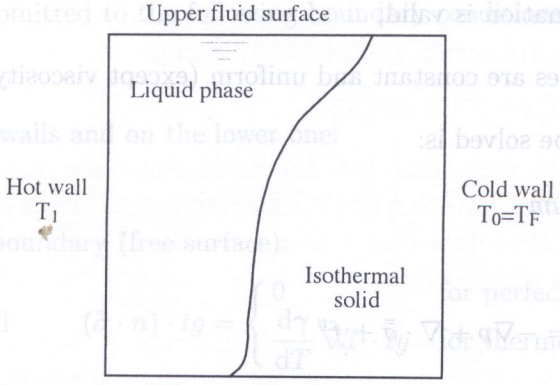

Fig. 1. Schematic diagram of the problem

boundary is assumed to be a free surface, with either perfect slipping or thermocapillary conditions. The free surface results are compared to the reference results of the benchmark, in order to show the significance of the Marangoni convection.

The thermophysical properties used (the same as the ones of Bertrand *et al.* [3], Gobin and Le Quéré, [17]) yield a Prandtl number of $Pr = 0.02$ ($Pr = \nu/\alpha$), a Stefan number of $Ste = 0.01$ ($Ste = C_P(T_1 - T_F)/L_F$) and a Rayleigh number of $Ra = 2.5 \cdot 10^5$ ($Ra = g\beta(T_1 - T_F)H^3/\alpha\nu$).

The thermocapillary aspect of the problem is characterized by the Marangoni number

$$Ma = \frac{\mathrm{d}\gamma}{\mathrm{d}T}(T_1 - T_F)\frac{H}{\mu\alpha} \tag{1}$$

where the surface tension γ is assumed to vary linearly with the temperature

$$\gamma = \gamma_{(T=T_F)} + \frac{\mathrm{d}\gamma}{\mathrm{d}T}(T - T_F) \tag{2}$$

For tin, the literature gives roughly $\mathrm{d}\gamma/\mathrm{d}T = -10^{-4}$ $\mathrm{Nm^{-1}K^{-1}}$, which yields a Marangoni number of $Ma = 1.25 \cdot 10^3$ and corresponds to a thermal Bond number of $Bo = Ra/Ma = 200$.

3. Model description

3.1. Governing equations

Our model is based on the finite element method and an enthalpy formulation fixed grid methodology. In the classification established by Voller *et al.* [48], it is the latent heat source method. That is, the energy equation is written in the classical convection-diffusion heat equation form with an additional source term in order to take into account the latent heat release or absorbing, depending on either solidification or melting has to be considered (Voller and Prakash [46]).

For an application to non-isothermal phase change, the momentum equations must be modified, in order to model the liquid flow in the mushy region. This can be done by adding a Darcy-like term in these equations (Voller and Prakash [46]), thus leading to the enthalpy-porosity approach (Brent *et al.* [4]). However, for the solidification or melting of a pure medium, the thickness of the mushy layer tends to zero. Therefore, such a modeling of inter-dendritic fluid flow is not needed. Actually, a temperature dependant viscosity, taking a very high value in the solid phase, is sufficient.

As for the benchmark, we have the following assumptions:

- the problem is two-dimensional;
- viscous dissipation is neglected;
- the flow in the liquid phase is laminar, incompressible and Newtonian;

- the Boussinesq approximation is valid;
- thermophysical properties are constant and uniform (except viscosity and surface tension).

So the set of equations to be solved is:

a) *continuity and momentum*

$$\nabla \cdot u = 0 \tag{3}$$

$$\rho_0 \left[\frac{\partial u}{\partial t} + (u \cdot \nabla) u \right] = -\nabla p + \nabla \cdot \bar{\bar{\sigma}} + f^v \tag{4}$$

Here u designates the velocity vector, p the pressure and ρ_0 the density at the reference temperature $T_0 = T_F$. For Newtonian fluids the viscous stress tensor is given by

$$\bar{\bar{\sigma}} = \mu \left[(\nabla \otimes u) + (\nabla \otimes u)^T \right] \tag{5}$$

where the dynamic viscosity takes a different value in the solid and liquid phases

$$\begin{aligned} \mu &= \mu_L = 6 \cdot 10^{-3} \text{ N s m}^{-2} && \text{if } T > T_F \\ \mu &= \mu_S = \mu_L \cdot 10^6 && \text{if } T \leq T_F \end{aligned} \tag{6}$$

With the Boussinesq approximation, the body force f^v writes

$$f^v = \rho_0 \left[1 - \beta (T - T_0) \right] g, \tag{7}$$

where β is the volumetric expansion coefficient and g the gravity acceleration vector.

b) *heat transfer*

$$\rho_0 C_P \left[\frac{\partial T}{\partial t} + (u \cdot \nabla) \right] = \nabla \cdot q + S^T. \tag{8}$$

Here T is the temperature, C_P the specific heat coefficient, and $q = -k \nabla T$ the heat flux (with k the thermal conductivity, thus $\alpha = k / \rho C_P$ is the thermal diffusivity). In this equation, the latent heat release is taken into account by the source term

$$S^T = -\rho_0 L_F \left[\frac{\partial f_L}{\partial t} + (u \cdot \nabla) f_L \right], \tag{9}$$

where $L_F = 6 \cdot 10^4$ Jkg^{-1} is the latent heat of melting and f_L the volume fraction of liquid. The latter, which is actually a step function for isothermal phase change, is modeled by

$$f_L = \begin{cases} 0 & \text{if } T < T_F - \varepsilon, \\ (T - T_F + \varepsilon) / 2\varepsilon & \text{if } T_F - \varepsilon \leq T \leq T_F + \varepsilon, \\ 1 & \text{if } T > T_F + \varepsilon, \end{cases} \tag{10}$$

where ε is a small parameter that controls the size of the mushy region. We have used $\varepsilon = 10^{-3}(T_1 - T_F)$.

This set of equations is submitted to the following boundary conditions:

a) *momentum*

– on the two vertical walls and on the lower one:

$$u = 0 \tag{11}$$

– on the fluid upper boundary (free surface):

$$u \cdot n = 0 \qquad \text{and} \qquad (\bar{\bar{\sigma}} \cdot n) \cdot tg = \begin{cases} 0 & \text{for perfect slipping} \\ \dfrac{\mathrm{d}\gamma}{\mathrm{d}T} \nabla T \cdot tg & \text{for thermocapillary convection} \end{cases} \tag{12}$$

where n and tg are respectively the external normal and the tangential vectors;

b) *heat transfer*

– on the two horizontal walls:

$$q \cdot n = 0, \tag{13}$$

– on the left vertical wall:

$$T = T_1\,, \tag{14}$$

– on the right vertical wall:

$$T = T_F\,. \tag{15}$$

3.2. Finite element formulation

The weak forms and the finite element formulations of the fluid flow problem (Eqs. (3)–(4)) and of the heat transfer one (Eq. (8)) are obtained following the standard procedure of the Galerkin finite element method (Gresho and Sani [19]) and will not be given in detail here.

Concerning the fluid flow problem, we have used a primary variables (u, p) formulation with a penalty approach. The space discretization is obtained with degrees of freedom are eliminated at the element level a quadratic approximation for the velocity and a piecewise linear disicontinous approximation for the pressure whose $Q_2 - P_{-1}$. The surface tension action appears in the weak form through a boundary integral. This part is discretized using a specific three-node boundary element as usual.

The weak form of the heat transfer problem is discretized in space with the C^0 rectangular four-nodes Lagrange element.

Both problems are integrated in time with the first order backward Euler scheme.

3.3. Solution strategy

At each time step, the two algebraic systems resulting from the finite element formulation of the fluid flow and heat transfer problems are solved separately, starting with the heat transfer one. The initial temperature and velocity fields are set to T_F and 0, respectively. Then, each problem uses the last available solution of the other one, but we do not loop between the two problems within a time step. Thus, the model is not fully implicit, leading to a limitation in the time step size. In practice this limitation is not penalizing in regard of the time scale of the process that we have to analyze.

Since the fluid flow system is non-linear we use the Newton linearization to solve it. Less than four iterations are almost needed.

The key point for the efficiency of the model lies in the solution strategy of the heat transfer equation. Let us write the corresponding algebraic system as

$$([M] + \Delta t\,[K])\,\{T\} = [M]\,\{T\}^{\text{old}} + \Delta t\,\{F\}\,, \tag{16}$$

where Δt is the value of the time step, $[M]$ the consistent mass matrix and $[K]$ the "stiffness" matrix taking into account the convection and conduction terms. $\{F\}$ is the "load" vector taking into account the contribution of the latent heat source term (9). $\{T\}$ is the unknown vector containing the nodal temperatures and $\{T\}^{\text{old}}$ contains the nodal temperatures obtained at the previous time step.

In the standard source term method, the liquid fraction f_L is considered as an independent variable. The algebraic system (16) is then linear, but iterations are needed (substitution algorithm), with updating of the liquid fraction, until the temperature is consistent with the current liquid fraction field (Voller *et al.* [48]). As noticed by Voller [44], the efficiency of this iterative approach can be greatly improved by considering more the temperature dependence of the source term in the formulation of the system. The Newton linearization is a natural and rigorous way to do this in a finite element framework (Storti *et al.*, [39]). The corresponding iterative procedure consists in solving at iteration $i+1$, the following system

$$[J]^i\,\{\Delta T\}^{i+1} = -\{R\}^i \qquad \text{with} \qquad \{\Delta T\}^{i+1} = \{T\}^{i+1} - \{T\}^i\,, \tag{17}$$

where $\{R\}$ is the residual vector

$$\{R\} = ([M] + \Delta t\,[K])\,\{T\} - [M]\,\{T\}^{\text{old}} - \Delta t\,\{F\}\,, \tag{18}$$

and $[J]$ is the Jacobian matrix

$$[J] = \frac{\partial\{R\}}{\partial\{T\}} = [M] + \Delta t\left([K] - \frac{\partial\{F\}}{\partial\{T\}}\right). \tag{19}$$

As noticed by Voller *et al.* [48], this builds a natural bridge between source based methods and apparent heat capacity methods. Actually, if in equation (19) the derivative of $\{F\}$ is computed exactly, the two methods are equivalent at the condition that the same approximation for f_L is used.

4. Results and discussion

Three kinds of boundary conditions at the upper liquid boundary have been considered, namely no slip, perfect slipping and surface tension gradient (Eq. (12)), whereas at the other walls of the cavity zero velocity has been taken. Thermal bounday conditions are given by Eqs. (13)–(15).

A uniform structured grid, made up of 200 × 100 (horizontal × vertical) quadrilateral finite elements (Q_9) and, a uniform time step of $\Delta t = 10^{-4}$ have been considered. The non-dimensional time is defined as *SteFo*, where $Fo = \alpha t/H^2$ is the Fourier number. Calculations have been continued up to $SteFo = 0.1$, which corresponds to 1000 time steps.

In the following, three types of results are provided to give a global view of the influence of the upper liquid boundary condition on the melting process. The isotherms and streamlines plotted, respectively in Figs. 2 and 3 at four different times of the process, give an overview of the heat transfer and the fluid flow structure in the liquid phase. Moreover, the Nusselt number distribution along the hot wall and the melting front position and its shape are provided in Figs. 4 and 5, respectively in order to compare the results to experimental or other numerical studies. Finally, Figs. 6 and 7 show time evolution of the average Nusselt number along the hot wall and of the volume liquid fraction. These last results can be compared to existing correlations, namely to Gobin and Benard's one [16] for the average Nusselt number, and to the classical solution of the Stefan problem [38] for the volume liquid fraction.

Fig. 2. Isotherms ($0 \leq T \leq 3$, $\delta T = 0.3$) at $SteFo = 0.004$, 0.01, 0.04 and 0.1; a) rigid upper wall, b) perfect slipping free surface, c) thermocapillary free surface

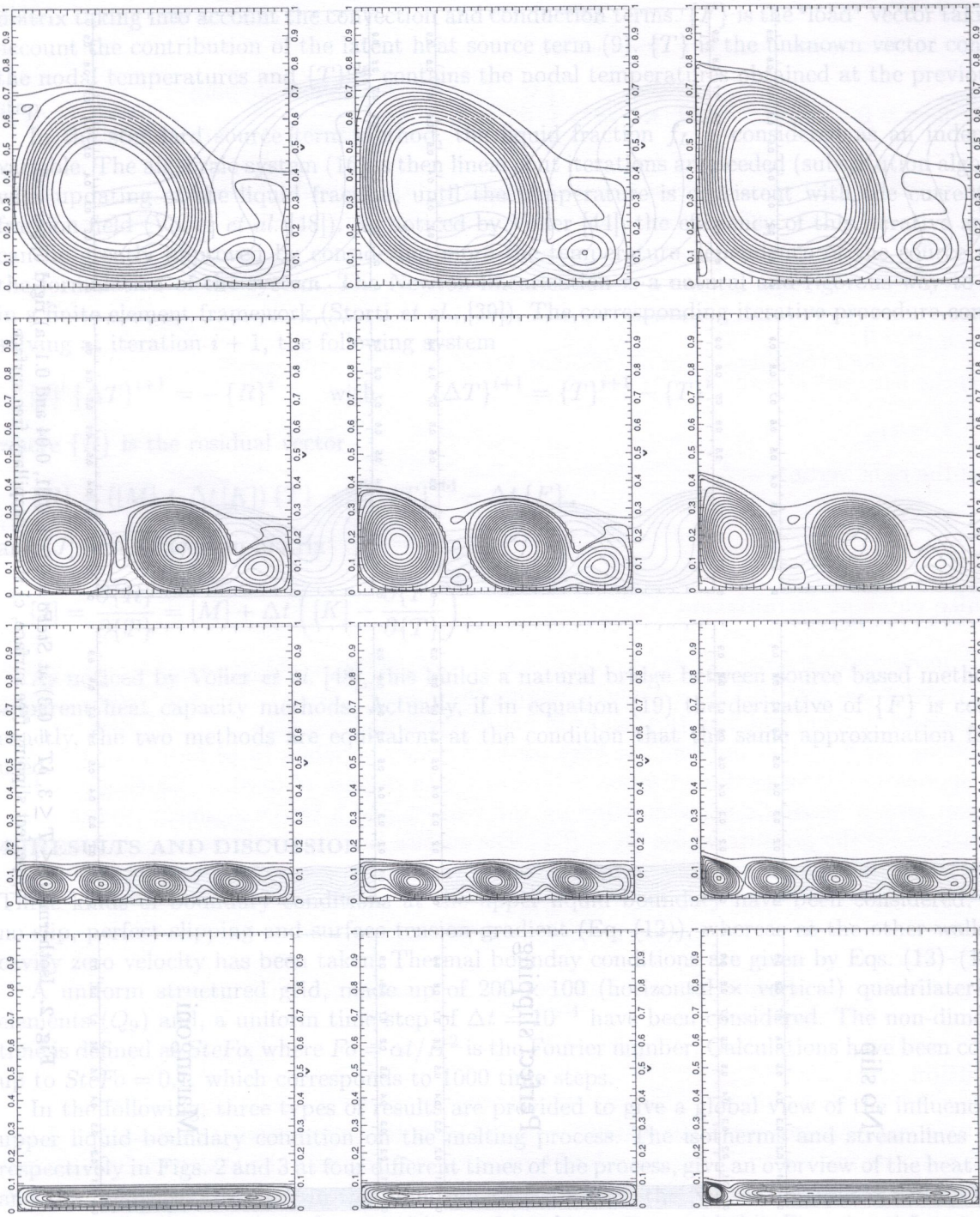

Fig. 3. Flow pattern (streamlines) at $SteFo = 0.004$, 0.04, 0.01 and 0.1; a) rigid upper wall, b) perfect slipping free surface, c) thermocapillary free surface

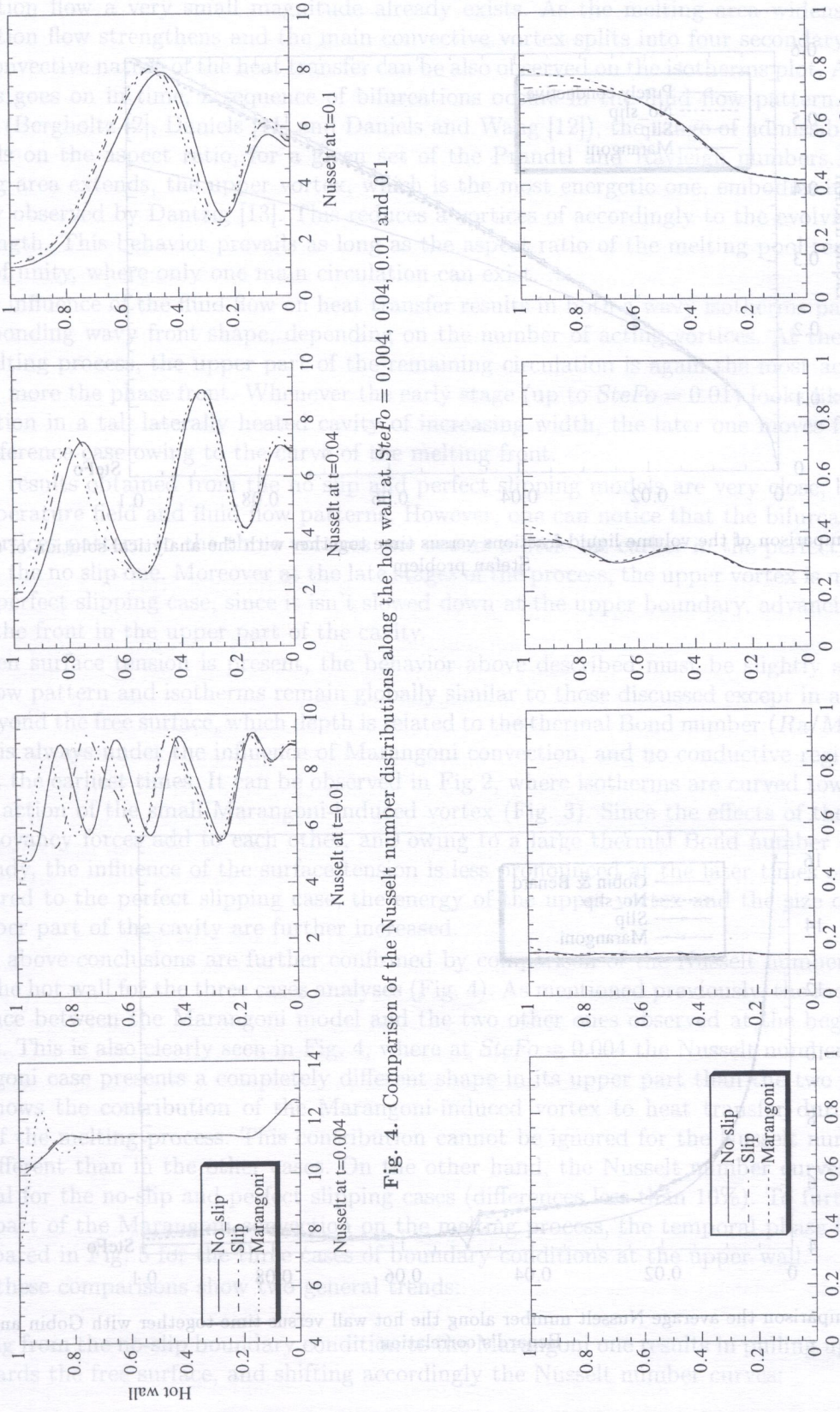

Fig. 4. Comparison of the Nusselt number distributions along the hot wall at $SteFo = 0.004$, 0.04, 0.01 and 0.1

Fig. 5. Comparison of the front locations and shape at $SteFo = 0.004$, 0.04, 0.01 and 0.1

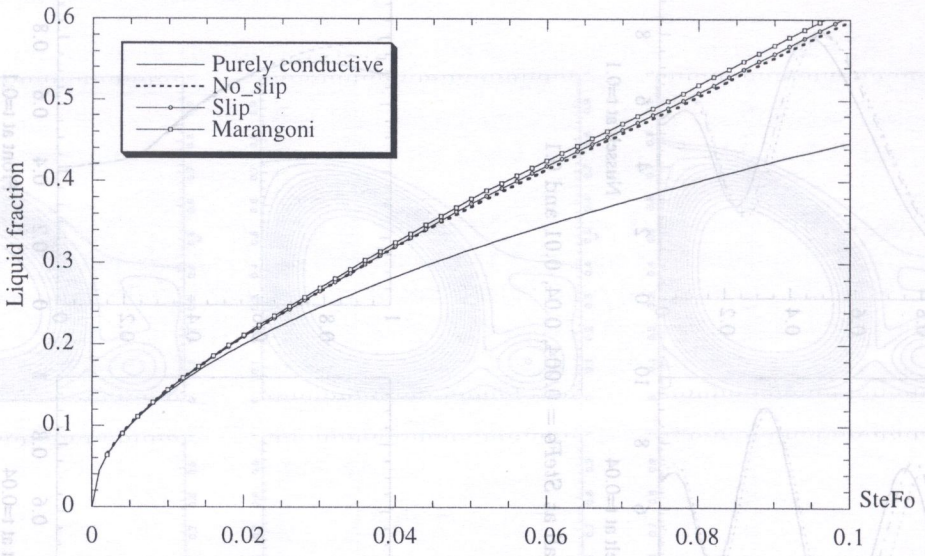

Fig. 6. Comparison of the volume liquid fractions versus time together with the analytical solution of the Stefan problem

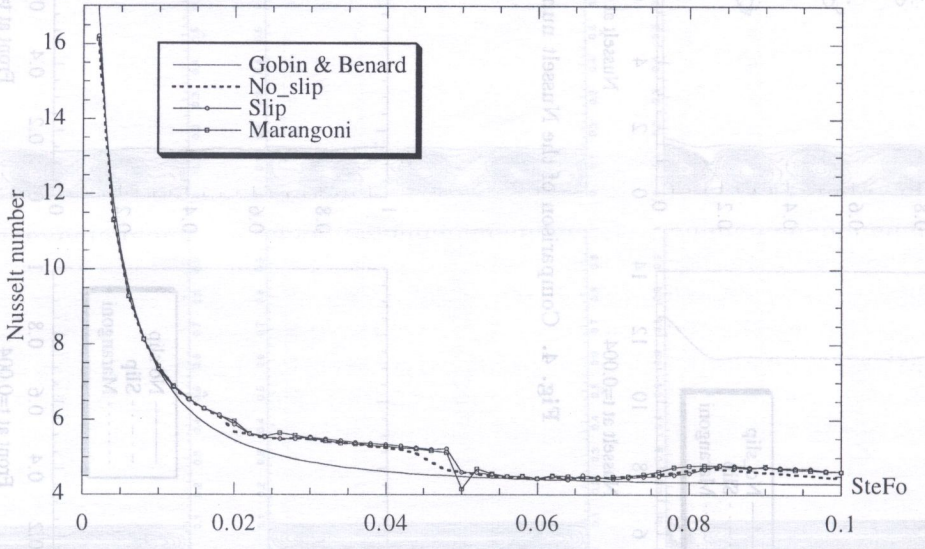

Fig. 7. Comparison the average Nusselt number along the hot wall versus time together with Gobin and Benard's correlation

The isotherms plotted in Fig. 2 and streamlines plotted in Fig. 3 show that two regimes can be distinguished. Up to $SteFo = 4 \cdot 10^{-3}$, the heat transfer is mainly conductive, however a natural convection flow a very small magnitude already exists. As the melting area widens, the natural convection flow strengthens and the main convective vortex splits into four secondary circulations. This convective nature of the heat transfer can be also observed on the isotherms plot. As the melting process goes on in time, a sequence of bifurcations occurs in the fluid flow pattern. As it is well known (Bergholtz [2], Daniels [11] and Daniels and Wang [12]), the range of admissible wavelength depends on the aspect ratio, for a given set of the Prandtl and Rayleigh numbers. Thus, as the melting area extends, the upper vortex, which is the most energetic one, embodies its neighbor as already observed by Dantzig [13]. This reduces a vortices of accordingly to the evolving admissible wavelength. This behavior prevails as long as the aspect ratio of the melting pool reaches its limit value of unity, where only one main circulation can exist.

The influence of the fluid flow on heat transfer results in both a wavy isotherms pattern and the corresponding wavy front shape, depending on the number of acting vortices. At the late stage of the melting process, the upper part of the remaining circulation is again the most active, bending further more the phase front. Whenever the early stage (up to $SteFo = 0.01$) looks like the thermal convection in a tall laterally heated cavity of increasing width, the later one moves far away from that reference case owing to the curve of the melting front.

The results obtained from the no slip and perfect slipping models are very close, both in terms of temperature field and fluid flow patterns. However, one can notice that the bifurcation from the four vortices pattern to the three vortices one occurs a little bit earlier in the perfect slipping case than in the no slip one. Moreover at the late stages of the process, the upper vortex is more energetic in the perfect slipping case, since it isn't slowed down at the upper boundary, advancing a little bit faster the front in the upper part of the cavity.

When surface tension is present, the behavior above described must be slightly adjusted. The fluid flow pattern and isotherms remain globally similar to those discussed except in a narrow layer just beyond the free surface, which depth is related to the thermal Bond number (Ra/Ma ratio). This region is always under the influence of Marangoni convection, and no conductive regime can exist, even at the earliest times. It can be observed in Fig 2, where isotherms are curved toward the right by the action of the small Marangoni-induced vortex (Fig. 3). Since the effects of thermocapillary and buoyancy forces add to each other, and owing to a large thermal Bond number considered in this study, the influence of the surface tension is less pronounced at the later times of the process. Compared to the perfect slipping case, the energy of the upper vortex and the size of the melt in the upper part of the cavity are further increased.

The above conclusions are further confirmed by comparison of the Nusselt number distribution along the hot wall for the three cases analyses (Fig. 4). As mentioned previously, the most significant difference between the Marangoni model and the two other ones observed at the beginning of the process. This is also clearly seen in Fig. 4, where at $SteFo = 0.004$ the Nusselt number curve in the Marangoni case presents a completely different shape in its upper part than the two other curves. This shows the contribution of the Marangoni-induced vortex to heat transfer during this early stage of the melting process. This contribution cannot be ignored for the Nusselt number is up to 40% different than in the other cases. On the other hand, the Nusselt number curves are roughly identical for the no-slip and perfect slipping cases (differences less than 10%). To further elucidate the impact of the Marangoni convection on the melting process, the temporal phase front position is compared in Fig. 5 for the three cases of boundary conditions at the upper wall.

All these comparisons show two general trends:

- going from the no-slip boundary condition to the Marangoni one results in pulling up the vortices towards the free surface, and shifting accordingly the Nusselt number curves;
- the perfect slipping model yields results that one bracketed by the two limiting cases of the no-slip and thermocapillary upper boundary conditions.

There is also interesting to notice that the change from the four-vortices pattern to the three-vortices one already takes place at $SteFo = 0.01$ for the perfect slipping case, and the Nusselt number displays three main waves instead of four (The second plot of Fig. 4, and Fig. 5).

The results displayed in Figs. 6 and 7 represent the integrated quantities, i.e. the total liquid fraction in the cavity and the average Nusselt number. No difference can be observed during the conductive regime between the three models. Concerning the volume liquid fraction, plotted versus time in Fig. 6, the values predicted by the three models are very close. In the Marangoni case the volume liquid fraction increases only 4% over other at the final computation ($SteFo = 0.1$). For again the perfect slipping case its value is between the two limiting cases. The evolution of the average Nusselt number, goes in a very similar way for all boundary cases and its values are close to the Gobin and Benard's correlation [16]. It is, however, noteworthy to notice that some deviations from this correlation exist. They appear between the change from the 3-vortex pattern to the 2-vortex one at $SteFo = 0.023$ and the between change from the 2-vortex pattern to the one-vortex structure at $SteFo = 0.05$. It seems that the sensitivity of the system to the three considered upper wall boundary conditions is very high in the latter case. Later on, the three models merge again towards the Gobin's correlation until $SteFo = 0.07$, where a new deviation can be observed. At the end of the computation time, the no-slip curve tends asymptotically to the correlation, whereas the perfect slipping and Marangoni models do not.

5. Conclusion

The influence of the free surface effects on the melting of a pure medium (tin) in a square cavity heated from one side has been numerically investigated. For this purpose, a model based on the finite element method and on the enthalpy formulation on a fixed grid has been developed.

The nature of the upper liquid boundary condition (no-slip, perfect slipping or thermocapillary) has little impact on the relevant integrated parameters of the melting process (average Nusselt number and volume liquid fraction). The differences observed between the three models are less than few percents for the considered cases, since the buoyancy remains dominant over the thermocapillary convection ($Bo = 200$). However a detailed analysis of the flow structure and the pertinent isotherm pattern reveals that the influence of the upper boundary condition is significant in a narrow layer adjacent to the free surface throughout the whole melting process. It has also been noticed that the upper boundary condition has an impact on the fluid flow dynamic, causing bifurcations between successive vortices.

Finally, this study shows that the developed, model based on a fixed grid methodology, is able to handle isothermal phase change problems with combined buoyancy and thermocapillary convections. A more comprehensive study, considering a wide range of the aspect ratio and of the thermal Bond number, would be very useful in order to determine when the thermocapillary effect must be taken into account in the thermal and/or fluid flow analysis. Furthermore, the understanding of many industrial processes (like metal casting, welding, surface processing, coating) could benefit from that study.

References

[1] B. Basu, J. Srinivasan. Numerical study of steady-state laser melting problem. *Int. J. Heat Mass Transfer*, **31**(11): 2331–2338, 1988.

[2] R.F. Bergholtz. Instability of steady natural convection in a vertical lot. *J. Fluid Mech.*, **84**: 743–768, 1978.

[3] O. Bertrand, B. Binet, H. Combeau, S. Couturier, Y. Delannoy, D. Gobin, M. Lacroix, P. Le Quéré, M. Medale, J. Mencinger, H. Sadat, G. Veirã. Melting driven by natural convection. A comparison exercise. *Int. J. of Therm. Sci.*, **38**: 5–26, 1999.

[4] A.D. Brent, V.R. Voller, K.J. Reid. Enthalpy-porosity technique for modeling convection-diffusion phase change: application to the melting of a pure metal. *Numer. Heat Transfer*, **13**: 297–318, 1988.

[5] R.A. Brown, T.A. Kinney, P.A. Sackinger, D.E. Bornside. Toward an integrated analysis of Cochralski growth. *J. Cryst. Growth*, **97**: 99–115, 1989.

[6] B.M. Carpenter, G.M. Homsy. Combined buoyant-thermocapillary flow in a cavity. *J. Fluid. Mech.*, **207**: 121–132, 1989.

[7] C. Chan, J. Mazumder, M.M. Chen. A two-dimensional transient model for convection in laser melted pool. *Metall. Trans. A*, **15A**: 2175–2184, 1984.

[8] K.C. Chiang, H.L. Tsai. Shrinkage-induced fluid flow and domain change in two-dimensional alloy solidification. *Int. J. Heat Mass Transfer*, **35**: 1763–1770, 1992.

[9] S. Chippada, T.C. Jue, B. Ramaswamy. Finite-element simulation of combined buoyancy and thermocapillary driven convection in open cavities. *Int. J. Num. Meth. Eng.*, **38**: 335, 1995.

[10] K.A. Cliffe, S.J. Tavener. Marangoni-Bénard convection with a deformable free surface. *J. Comp. Phys.*, **145**: 193–227, 1998.

[11] P.G. Daniels. Transition to the convective regime in a vertical slot. *Int. J. Heat Mass Transfer*, **28**: 2071–2077, 1985.

[12] P.G. Daniels, P. Wang. Numerical study of thermal convection in tall laterally heated cavities. *Int. J. Heat Mass Transfer*, **37**: 375–386, 1994.

[13] J.A. Dantzig. Modeling liquid-solid phase changes with melt convection. *Int. J. Num. Meth. Eng.*, **28**: 1769–1785, 1989.

[14] M.C. Fleming. *Solidification Processing.* McGraw-Hill, New York, 1974.

[15] C. Gau, R. Viskanta. Melting and solidification of a pure metal on a vertical wall. *J. Heat Transfer*, **108**: 174–181, 1986.

[16] D. Gobin, C. Benard. Melting of metals driven by natural convection in the melt: influence of the Prandtl and Rayleigh numbers. *J. Heat Transfer*, **114**: 521–524, 1992.

[17] D. Gobin, P. Le Quéré. Melting in enclosures: Coupled heat transfer and natural convection. In: Kowalewski, Stella, Banaszek, Szmyd, eds., *ESF-AMIF Workshop on Phase Change with Convection, Modeling and Validation*, 13–18, 1999.

[18] G. Gousbet, J. Maquet, C. Roze, R. Darrigo. Surface tension and coupled buoyancy-driven instability in a horizontal liquid layer: overstability and exchange of stability. *Phys. Fluids A*, **2**(6): 903–911, 1990.

[19] P.M. Gresho, R.L. Sani. *Incompressible flow and the finite element method – Advection-diffusion and isothermal laminar flow.* John Wiley and Sons, Chichester, 1998.

[20] B.H. Hadid, B. Roux. Buoyancy- and thermocapillary-driven flows in a shallow open cavity: unsteady flow regimes. *J. Cryst. Growth*, **97**: 217–225, 1989.

[21] Y.F. Hsu, B. Rubinsky. Two-dimensional heat transfer study on the keyhole plasma arc welding process. *Int. J. Heat Mass Transfer*, **31**(7): 1409–1421, 1988.

[22] A.D.W. Jones. Hydrodynamics of Czochralski growth – a review of the effects of rotation and buoyancy forces. *Prog. Cryst. Growth Charact.*, **9**: 139–168, 1984.

[23] Y. Katsumura, H. Hashizume, S. Toda. Numerical analysis of fluid flow with free surface and phase change under electromagnetic force. *IEEE Trans. Magnetics*, **32**(3): 1002–1005, 1996.

[24] R.G. Keanini, B. Rubinsky. Three-dimensional simulation of the plasma arc welding process. *Int. J. Heat Mass Transfer*, **36**(13): 3283–3298, 1993.

[25] A.G. Kirdyashkin. Thermogravitational and thermocapillary flows in a horizontal liquid layer under the conditions of a horizontal temperature gradient. *Int. J. Heat Mass Transfer*, **27**(8): 1205–1218, 1984.

[26] N. Kobayashi. Hydrodynamics in Czochralski growth-computer analysis and experiments. *J. Crystal Growth*, **52**: 425–434, 1981.

[27] S. Kou, Y.H. Wang. Weld pool convection and its effect. *Welding Research Supplement*, 63-s–70-s 1986,.

[28] C.W. Lan, S. Kou. Thermocapillary flow and natural convection in a melt column with an unknown melt/solid interface. *Int. J. Num. Meth. Fluids*, **12**: 59–80, 1991.

[29] A. Liu, T.E. Voth, T.L. Bergman. Pure material melting and solidification with liquid phase buoyancy and surface tension forces. *Int. J. Heat Mass Transfer*, **36**(2): 411–422, 1993.

[30] M.A. McClelland. Time-dependent liquid metal flows with free convection and a deformable free surface. *Int. J. Num. Meth. Fluids*, **20**: 603–620, 1995.

[31] M. Medale, M. Jaeger. Modélisation par éléments finis d'écoulements à surface libre avec changement de phase solide-liquide. *Int. J. Therm. Sci.*, **38**: 267–276, 1999.

[32] G.M. Oreper, J. Szekely. Heat- and fluid-flow phenomena in weld pools. *J. Fluid Mech.*, **147**: 53–79, 1984.

[33] K. Ravindran, J. Srinivasan, A.G. Marathe. Finite element study on the role of convection in laser surface melting. *Numer. Heat Transfer Part A*, **26**: 601–618, 1994.

[34] A.A. Samarskii, P.N. Vabishchevich, O.P. Iliev, A.G. Churbanov. Numerical simulation of convection/diffusion phase change problems – a review. *Int. J. Heat Mass Transfer*, **36**(17): 4095–4106, 1993.

[35] G.P. Sasmal, J.I. Hochstein. Marangoni convection with a curved and deforming free-surface in a cavity. *J. Fluids Eng.*, **116**: 577–588, 1994.

[36] D. Schwabe. Marangoni effects in crystal growth metals. *Phys.-Chem. Hydro.*, **2**: 263–280, 1981.

[37] W. Shyy, M.-H. Chen. A study of the transport process of buoyancy-induced and thermocapillary flow of molten alloy. *Comp. Meth. Applied Mech. Eng.*, **105**: 333–358, 1993.

[38] J. Stefan. Über die Theorie des Eisbildung, insbesonder über die Eisbildung im Polarmeere. *J. Ann. Phys. Chem.*, **42**: 269–286, 1891,.

[39] M. Storti, L.A. Crivelli, S. Idelsohn. An efficient tangent scheme for solving phase-change problems. *Comp. Meth. Applied Mech. Eng.*, **66**: 65–86, 1988.

[40] M.C. Tsai, S. Kou. Marangoni convection in weld pools with a free surface. *Int. J. Num. Meth. Fluids*, **9**: 1503–1516, 1989.

[41] D. Villers, J.K. Platten. Separation of Marangoni convection from gravitational convection in earth experiments. *PhysicoChem. Hydrodynam.*, **8**(2): 173–183, 1987.

[42] D. Villers, J.K. Platten. Coupled buoyancy and Marangoni convection in acetone: experiments and comparison with numerical simulations. *J. Fluid. Mech.*, **234**: 487–510, 1992.

[43] R. Viskanta. Natural convection in melting and solidification. In: S. Kakac, W. Aung, R. Viskanta, eds., *Natural convection; fundamentals and applications.* Hemisphere, New York, 845–877, 1985.

[44] V.R. Voller. Fast implicit finite-difference method for the analysis of phase change problems. *Numer. Heat Transfer Part B*, **17**: 155–169, 1990.

[45] V.R. Voller. An overview of numerical methods for solving phase change problems. *Adv. Num. Heat Transfer*, Vol. **1**, 341–380. Taylor and Francis, 1997.

[46] V.R. Voller, C. Prakash. A fixed grid numerical modeling methodology for convection-diffusion mushy region phase-change problems. *Int. J. Heat Mass Transfer*, **30**(8): 1709–1719, 1987.

[47] V.R. Voller, S. Sundarraj. A model of inverse segregation: the role of microporosity. *Int. J. Heat Mass Transfer*, **38**(6): 1009–1018, 1995.

[48] V.R. Voller, C.R. Swaminathan, B.G. Thomas. Fixed grid techniques for phase change problems: a review. *Int. J. Num. Meth. Eng.*, **30**: 875–898, 1990.

[49] T. Zacharia, S.A. David, J.M. Vitek. Effect of convection on weld pool development. In: M.J. Cieślak, J.H. Perepeczko, S. Kang, M.E. Glicksman, eds., *The Metal Science of Joining*, 257–263. The Minerals Metals and Materials Society, 1992.